Supplement of Biogeosciences, 20, 1635–1648, 2023
https://doi.org/10.5194/bg-20-1635-2023-supplement

Biogeosciences Open Access EGU

Supplement of

Long-term changes of nitrogen leaching and the contributions of terrestrial nutrient sources to lake eutrophication dynamics on the Yangtze Plain of China

Qi Guan et al.

Correspondence to: Jing Tang (jing.tang@nateko.lu.se)

Section S1 Regrouping land cover fractions

Annual land cover fractions of urban, cropland, pasture and natural area were derived from the 37 land cover types in the Climate Change Initiative Land Cover (CCI-LC version 2.0) dataset (Defourny et al., 2012) with a spatial resolution of 300m. For a given 0.1° grid cell, we determined all original land cover class pixels within this grid cell, which were then grouped into urban, cropland, pasture and natural area according to the guideline of CCI-LC dataset (Kirches et al., 2014). The cover fractions of each land use type were calculated as the number of pixels in the land use type divided by the total number of pixels within one 0.1 grid cell, which were used as input datasets for LPJ-GUESS.

Section S2 Interpolation of crop distribution maps

The crop cultivation maps in Yangtze Plain were interpolated from station-based observations by using an adaptive inverse distance weighting method (AIDW) (Lu and Wong, 2008). In this study, we assumed that the two nearest fields stations for a given grid cell provide critical information about crop types and corresponding planting fractions for gridded crop cultivation maps. The crop planting fractions were related to inverse-distance weights modified by optimal decay parameters, which were derived adaptively based on spatial distributions of field stations across Yangtze Plain. For a given point, the spatial pattern coefficient (R), representing spatial distributions, was determined as the ratio between the actual (r_{obs}) and expected (r_{exp}) nearest neighbor distance. The numbers of field stations (n) and the total area of Yangtze Plain (A) were used to calculate the expected nearest neighbor distance (r_{exp}) according to the following formula (Lu and Wong, 2008).

$$r_{exp} = 1/(2(n/A)^{0.5}) \quad \text{(S.1)}$$

Similarly, the nearest neighbor distance (r_{obs}) was also calculated based on the two nearest field stations. To assign the optimal decay parameters, the spatial pattern (R) was required to be normalized by using min-max normalization.

$$\mu_R = \begin{cases} 0, & R(S_0) < R_{\min} \\ 0.5 + 0.5\sin(\pi/R_{\max})(R(S_0) - R_{\min}), & R_{\min} \le R(S_0) \le R_{\max} \\ 1, & R(S_0) > R_{\max} \end{cases} \quad \text{(S.2)}$$

The optimal decay parameters (α) were then converted from normalized spatial pattern (μ_R) based on Fig. 3 in (Lu and Wong, 2008). Finally, the exponential function with the optimal decay parameters was used to derive inverse-distance weights as crop planting fractions, thus producing gridded crop types and planting fraction maps for Yangtze Plain (Fig. S3).

Section S3 Recalibrating the parameters of rice-related CFTs

Based on the observed of crop yield, we recalibrated the relationship between the leaf-based nitrogen content and the maximum catalytic capacity of rubisco, and this relationship can be expressed as.

$$N = pV_m^{25} + N_0 \quad (1)$$

where N represents the foliage nitrogen content; V_m^{25} is the maximum catalytic capacity of rubisco at 25℃; p and N_0 are the empirical coefficients. Moreover, the larger leaf area characterizes the hybrid and super-hybrid rice (Huang et al., 2020). In such case, we set the different combinations of parameter p (i.e., 1-25) and specific leaf area (SLA: 40-70) and then simulated the crop yield for the rotation of early- and late-season rice and single-season rice. The simulated crop yield was compared with the observed values, from which the pairs of parameter p and SLA corresponding to the lowest relative mean error was obtained as the optimal parameters used in the simulations of the whole Yangtze Plain.

Table S1. Basic information (names and crop rotations) and relevant parameters (CFTs, hydrology, specific leaf area (SLA, unit: m^2/kg C), empirical parameter expressing relationship between leaf N and maximum Rubisco capacity, *p* and harvest efficiency) of eleven studied crop types in agricultural ecosystems of Yangtze Plain, where three types of hydrological managements were used here, including irrigation till saturation (irrigated_sat), inundation (inundated) and rain-fed (rainfed).

CFTs	Crop names	Rotations	Hydrology	SLA	*p*	Harvest efficiency
TeCoWWi	summer maize, winter wheat	Yes	irrigated_sat	45, 35	25, 25	0.9, 0.9
TeSoWWi	soybean, winter wheat	Yes	irrigated_sat	30, 35	25, 25	0.9, 0.9
TrELRi	early-, late-season rice	Yes	inundated	55, 70	4, 3	1.0, 1.0
TrSRi	single-season rice	No	inundated	45	4	1.0
TrPe	peanut	No	irrigated_sat	45	25	0.9
TeSWi	spring wheat	No	irrigated_sat	35	25	0.9
TeSc	sugar cane	No	rainfed	45	25	0.9
TeWWi	winter wheat	No	irrigated_sat	35	25	0.9
TeRa	rapeseed	No	irrigated_sat	30	25	0.9
TeCoSp	spring maize	No	irrigated_sat	45	25	0.9
TeSo	soybean	No	irrigated_sat	30	25	0.9

Table S2. Basic information (ID, names, locations, lake areas and catchment areas) and the mean PEO derived from satellite observation in fifty large lakes of Yangtze Plain.

ID	Name	Lon	Lat	Lake area (km^2)	Catchment area (km^2)	PEO (%)
L01	Beimin	111.87	29.71	14.25	919.08	88.52
L02	Xihu	111.94	29.36	40.00	2711.25	91.07
L03	Shanpo	112.03	29.43	18.83	2017.21	89.12
L04	Changhu	112.4	30.44	114.03	5771.52	87.01
L05	Datong	112.51	29.21	83.10	3638.43	75.43
L06	Donghu (CD)	112.64	29.37	24.85	232.47	89.48
L07	Dongting	113.12	29.34	2614.36	270662.3	69.73
L08	Honghu	113.34	29.86	340.05	4200.21	89.84
L09	Longsai	113.51	30.84	9.34	1443.24	87.64
L10	Huanggai	113.55	29.7	59.47	2510.91	94.81
L11	Wuhu (XT)	113.8	30.18	32.93	440.37	86.50
L12	Yezhu	114.07	30.86	25.88	1747.26	92.03
L13	Xiliang	114.08	29.95	28.58	918.27	90.53
L14	Luhu	114.2	30.22	47.33	790.83	83.38
L15	Futou	114.23	30.02	141.22	1494.63	87.58
L16	Houhu	114.28	30.74	12.61	876.63	85.61
L17	Tangxun	114.36	30.42	44.83	578.97	90.25
L18	Donghu (WH)	114.4	30.56	34.35	208.17	89.94
L19	Wuhu (WH)	114.49	30.81	27.5	3051.45	89.20
L20	Liangzi	114.51	30.23	351.77	3152.7	79.88
L21	Baoxie	114.58	30.38	17.75	2407.77	94.65
L22	Zhangdu	114.7	30.65	36.24	2413.44	91.88
L23	Baoan	114.71	30.25	38.71	512.01	84.87
L24	Wusi	114.71	30.45	12.00	599.04	91.71
L25	Yaer	114.72	30.46	12.64	3152.7	86.94
L26	Sanshan	114.77	30.31	17.83	662.4	89.96
L27	Daye	115.1	30.1	73.65	1247.31	89.09
L28	Wanghu	115.33	29.87	42.87	1258.11	81.86
L29	Wushan	115.59	29.91	15.11	1520.19	95.98
L30	Chihu	115.69	29.78	35.9	2069.23	91.44
L31	Taibai	115.81	29.97	27.42	1460.19	93.47
L32	Saihu	115.85	29.69	53.33	2523.69	87.68
L33	Xiayao	116.06	28.69	16.1	190.8	94.85
L34	Longgan	116.15	29.95	280.48	3233.07	83.85
L35	Poyang	116.67	29.14	3206.98	170502	78.12

L36	Wuchang	116.69	30.28	112.02	874.53	91.45
L37	Caizi	117.07	30.8	171.59	4015.98	90.26
L38	Shengjin	117.07	30.38	96.09	1639.98	92.76
L39	Baidang	117.38	30.81	38.69	1099.35	85.54
L40	Chaohu	117.53	31.57	786.01	12951.81	83.06
L41	Shijiu	118.88	31.47	178.04	1089	91.04
L42	Gucheng	118.92	31.28	27.9	1383.39	86.15
L43	Nanyi	118.96	31.11	197.83	4004.82	89.33
L44	Changdang	119.55	31.62	84.33	678.06	94.83
L45	Xijiu	119.8	31.37	11.18	567.45	93.36
L46	Gehu	119.81	31.6	139.56	1729.89	95.87
L47	Taihu	120.19	31.2	2537.17	18769.77	73.37
L48	Yangcheng	120.77	31.43	123.6	1556.1	83.95
L49	Chenghu	120.82	31.21	37.11	215.01	83.32
L50	Dianshan	120.96	31.12	63.71	2634.12	79.23

Table S3. N-P ratios of animal manure contained in global N manure products (Parham et al., 2003; Sheppard, 2019; Azeez and Van Averbeke, 2010).

	Cattle	Pig	Goat and sheep	Chicken and duck
N-P ratio	3.3:1	4.3:1	5.19:1	2.53:1

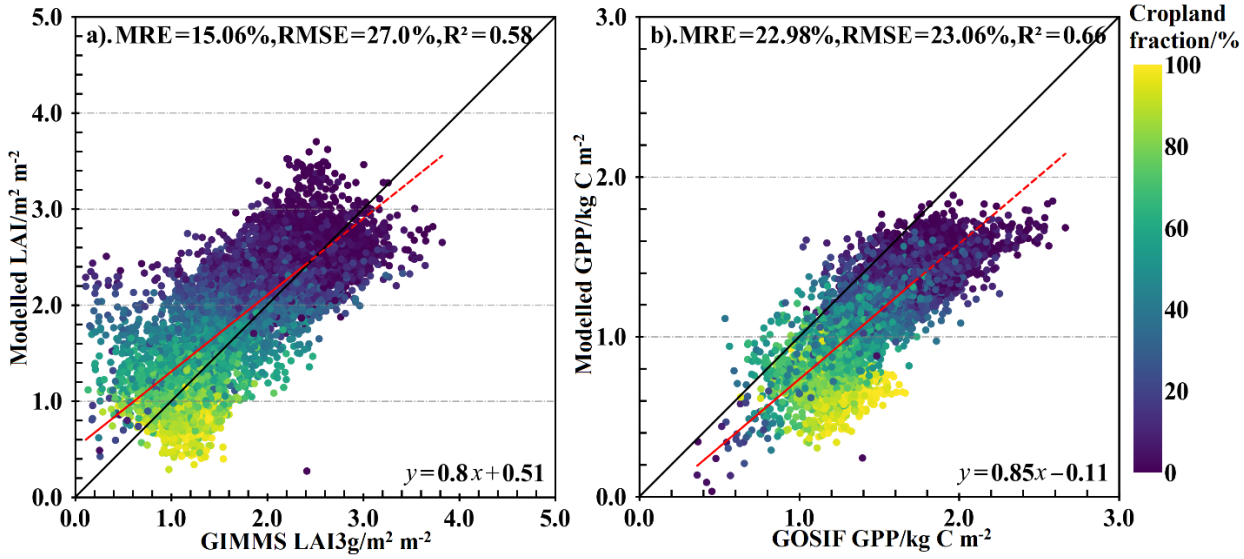

Figure S1. Comparison of the simulated LAI with GIMMS LAI3g from 1982 to 2011 **(a)** and modeled GPP against GOSIF GPP from 1992 to 2018 **(b)**, respectively. The red dashed lines are the fitting lines for the modeled with satellite-derived values.

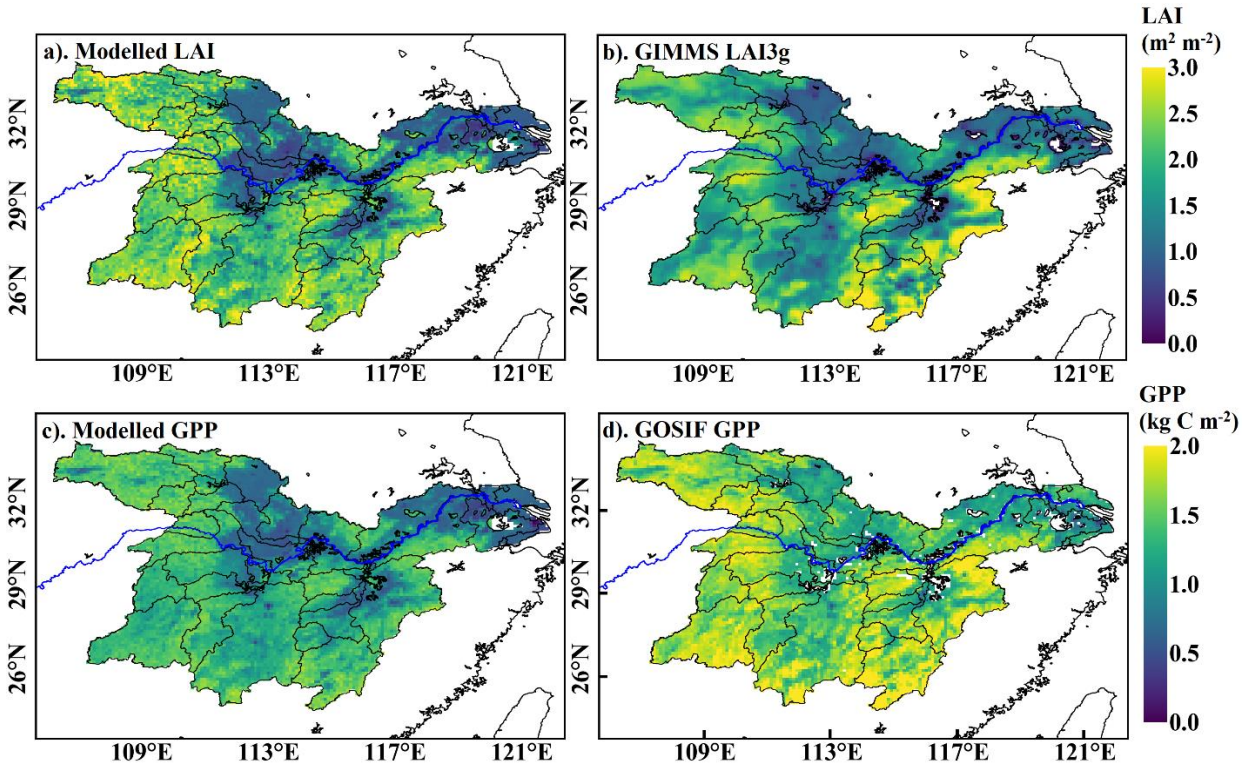

Figure S2. Comparison of spatial distributions for annual mean simulated LAI **(a)** v.s. LAI3g **(b)** for 1982-2011, and of simulated GPP **(c)** vs. GOSIF GPP **(d)** for 1992-2018.

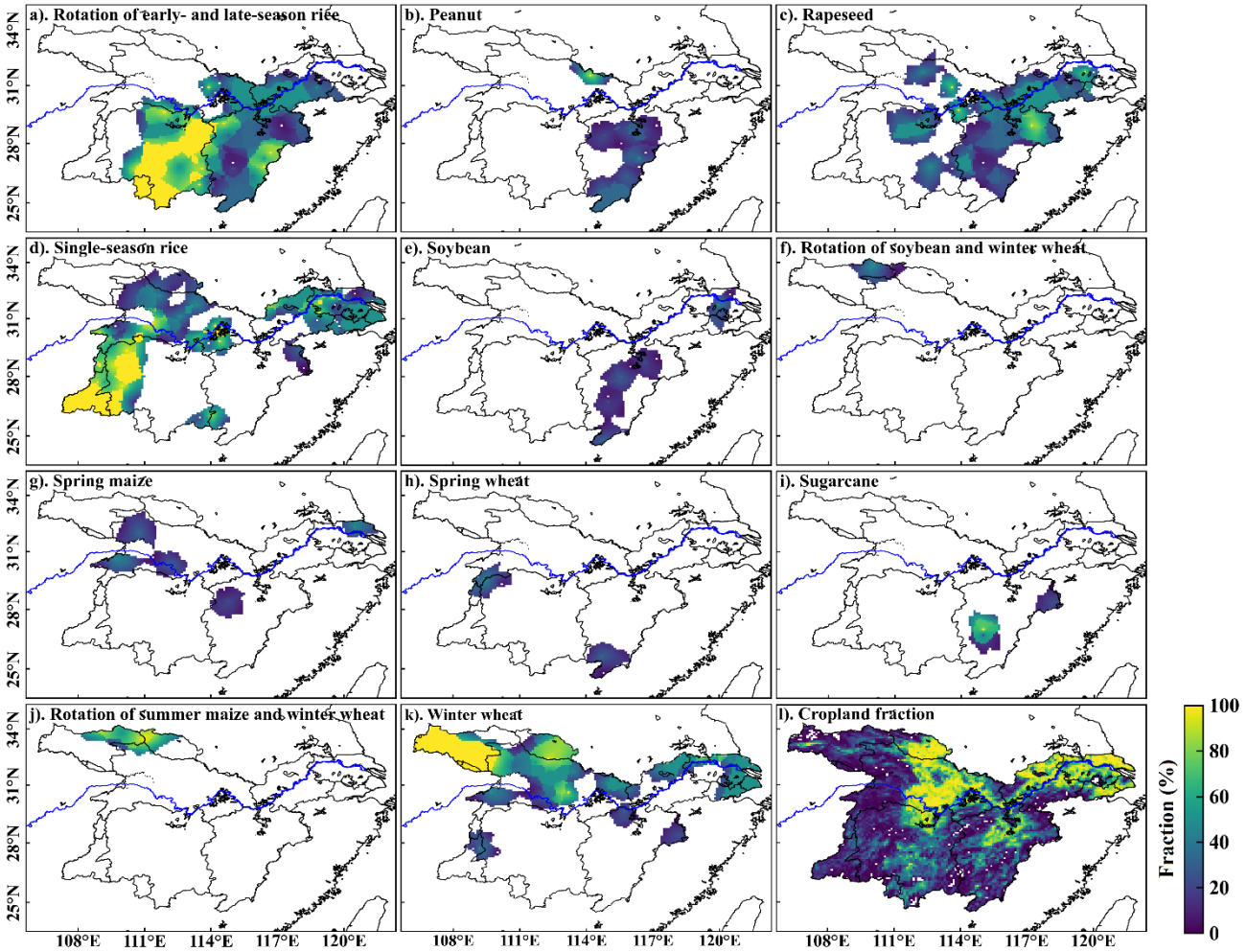

Figure S3. Spatial distributions of all studied cropland fraction for the crop types and crop rotations applied in the LPJ-GUESS simulation in Yangtze Plain. **a-k** represent the cropland fraction of each crop type against the cropland area. **i** shows the fraction of cropland over total land area.

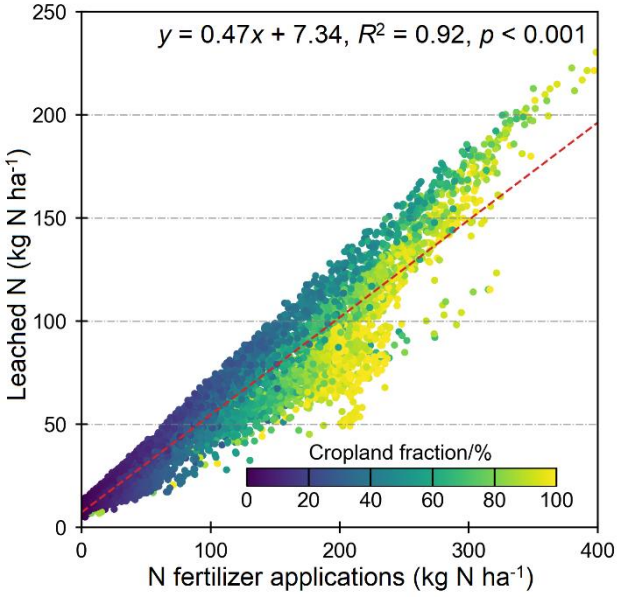

Figure S4. Response of leached nitrogen to different levels of fertilizer applications from 1979 to 2018 over the

entire Yangtze Plain.

References

Azeez, J. O. and Van Averbeke, W.: Nitrogen mineralization potential of three animal manures applied on a sandy clay loam soil, Bioresour Technol, 101, 5645-5651, 10.1016/j.biortech.2010.01.119, 2010.

Defourny, P., Kirches, G., Brockmann, C., Boettcher, M., Peters, M., Bontemps, S., Lamarche, C., Schlerf, M., and Santoro, M. J. P. U. G. V.: Land cover CCI, 2, 2012.

Huang, M., Lei, T., Cao, F., Chen, J., Shan, S., and Zou, Y.: Grain yield responses to nitrogen rate in two elite double-cropped inbred rice cultivars released 41 years apart, Field Crops Research, 259, 107970, 2020.

Kirches, G., Brockmann, C., Boettcher, M., Peters, M., Bontemps, S., Lamarche, C., Schlerf, M., Santoro, M., and Defourny, P.: Land cover cci-product user guide-version 2, ESA Public Document CCI-LC-PUG, 2014.

Lu, G. Y. and Wong, D. W.: An adaptive inverse-distance weighting spatial interpolation technique, Computers & Geosciences, 34, 1044-1055, 10.1016/j.cageo.2007.07.010, 2008.

Parham, J. A., Deng, S. P., Da, H. N., Sun, H. Y., and Raun, W. R.: Long-term cattle manure application in soil. II. Effect on soil microbial populations and community structure, Biology and Fertility of Soils, 38, 209-215, 10.1007/s00374-003-0657-7, 2003.

Sheppard, S. C.: Elemental Composition of Swine Manure from 1997 to 2017: Changes Relevant to Environmental Consequences, J Environ Qual, 48, 164-170, 10.2134/jeq2018.06.0226, 2019.